Multimodal vibration damping of a three-dimensional circular ring coupled to analogous piezoelectric networks

Alan Luo, Boris Lossouarn, Alper Erturk

Journal of Sound and Vibration 581 (2024) 118385

Contents lists available at ScienceDirect

Journal of Sound and Vibration

journal homepage: www.elsevier.com/locate/jsvi

Multimodal vibration damping of a three-dimensional circular ring coupled to analogous piezoelectric networks

Alan Luo [a], Boris Lossouarn [b,*], Alper Erturk [a]

[a] G.W. Woodruff School of Mechanical Engineering, Georgia Institute of Technology, 771 Ferst Dr NW, Atlanta, 30313, GA, USA
[b] Laboratoire de Mécanique des Structures et des Systèmes Couplés, Conservatoire national des arts et métiers, 292 rue Saint Martin, Paris, 75003, Île-de-France, France

ARTICLE INFO

Keywords:
Multimodal damping
Vibration control
Piezoelectric coupling
Electrical networks
Electromechanical analogy
Circular rings
Torsion
Bending
Shear deformation
Rotary inertia

ABSTRACT

Analogous piezoelectric networks have been shown to be effective for multimodal vibration attenuation in structures, including beams, plates, and rings. Previous studies for rings have only accounted for in-plane transverse vibration attenuation and disregarded the out-of-plane vibration modes. Furthermore, these previous numerical models and experiments have only been studied on thin rings, which ignore the effects of shear deformation and rotary inertia. As a result, these networks are not suitable for attenuating vibrations in thick rings. This study enhances on the previous electrical networks, considering both shear deformation and rotary inertia for both in-plane and out-of-plane vibrations. A new passive network topology is developed for the out-of-plane dynamics of thick rings, and the existing passive analogous network of in-plane vibration of thin rings is enhanced by considering the effects of shear deformation and rotary inertia. Combined, these new networks are capable of multimodal vibration damping of a thick ring in three-dimensions, encompassing primarily six types of vibration modes: the inextensional bending modes, the extensional modes, the thickness-shear modes, the coupled twist-bending modes, the torsional modes, and the transverse thickness-shear modes. By using piezoelectric elements to couple two separate analogous passive electrical networks derived from both the in-plane and out-of-plane governing equations of a ring and optimizing the internal resistance in each unit cell, it becomes possible to replicate the dynamics and effectively attenuate different types of vibration modes. This study serves as a theoretical foundation for implementations of passive vibration attenuation in ring structures.

1. Introduction

Vibration reduction has long been a topic of significant interest and importance in various industries. Circular symmetric structures such as rings, as essential components of many mechanical systems, are prone to generating vibrations either due to structural loading or due to dynamic operations in turbo-machinery [1]. Excessive vibrations contributes to increased wear, noise, and even structural damage. Previous studies have explored the dynamics of rotating rings at high speeds [2] as well as a comprehensive overview of rings in application to rolling tires [3]. Practical applications of vibration attenuation in circular rings have also been studied in gears [4,5]. Other applications have been studied in power transformers, where vibrations in the coil

* Corresponding author.
E-mail address: boris.lossouarn@lecnam.net (B. Lossouarn).

https://doi.org/10.1016/j.jsv.2024.118385
Received 19 October 2023; Received in revised form 5 March 2024; Accepted 6 March 2024
Available online 11 March 2024

winding are one of the main contributor to transformer noise, especially at high capacity loads [6]. This phenomenon was modeled mechanically using a series of stacked rings [7].

The dynamics of thin rings have been studied as early as the 1890s by Love [8]. Since then, various authors using different mathematical models have improved the original formulation, incorporating considerations for shear deformation and rotary inertia to accurately model thick rings for both in-plane and out-of-plane vibrations [9–12]. Other formulations include effects of rotation [13], and more recently, rotating rings derived from toroidal shell theory [14]. In this study, we focus on the vibration control of thick rings using an analogous electrical network derived from the governing equations of thick rings, aiming to develop a novel approach that addresses the unique dynamics posed by these structures.

The emergence of piezoelectric network damping in the early 2000s was driven by the desire to couple a structure to a medium that shares similar wave propagation properties [15]. However, the concept of electrical networks representing mechanical structures is not new. Analogous electrical networks were developed as early as the 1940s by MacNeal for beams [16], plates [17], stiffened shells [18], and entire aerospace structures [19]. These electrical networks were implemented and validated as a computational method for determining structural responses, but not as a method for piezoelectric vibration damping. Later, these electrical networks were independently theorized and developed specifically for vibration control, as they demonstrated optimal electromechanical coupling [20,21]. Circuit analogues were theorized for beams [22] and thin plates [23,24], but they were never realized due to the complex circuit topology.

To simplify and redesign the electrical networks, a finite difference scheme was applied to the classical mechanical equations of motion, which reduced the number of components required for assembly [25,26]. The use of magnetic components in these previous studies enabled the implementation of fully passive analogous networks. The analogous electrical networks are observed to have operational mode shapes resembling mechanical structures. By coupling the electrical network to a mechanical structure using piezoelectric patches, vibration damping applications can be achieved. The matching mode shapes between the electrical and mechanical domains enable the network to function as a vibration absorber at every point on the structure. Numerical and experimental validation of this approach was successfully carried out on rods [27], beams [25], and plates [26]. The network for a curved beam was developed [28] and then experimentally validated when assembled to form a network for thin rings [29]. The addition of curvature in a structure is reflected in the added complexity in the equations of motion due to the coupling between the circumferential displacements and transverse displacements, and thus, complicating the topology of the electrical network. Recently, the networks for beams and plates have been further enhanced to account for shear deformation and rotary inertia of the structure, commonly referred to as the Timoshenko-Ehrenfest beam [30] and the Mindlin-Reissner plate [31]. These modifications incorporate additional capacitance and inductance in the network that are analogous to shear deformation and rotary inertial effects. This enhancement improves the frequency coherence between the analogous electrical networks and beams and plates, which leads to improved vibration attenuation of these structural elements with thicker cross sections [32].

Using the network derived from the dynamics of curved beams, multimodal vibration damping of thin rings have been explored [29], showing significant vibration attenuation for in-plane inextensional bending modes numerically and experimentally. However, the electrical network used in this study for piezoelectric vibration damping does not account for the shear deformation and rotary inertia of the structure. As a result, the same network would not be optimal for thicker rings, which require additional considerations such as extension of the neutral axis, transverse shear, and rotary inertia [10,33]. Furthermore, the previous study only includes the damping of inextensional bending modes, which only account for a portion of the types of vibration modes exhibited by rings. Rings typically exhibit six types of modes, three of which are in-plane, the other three are out-of-plane modes [5,9,34]. The three in-plane mode types are the inextensional bending modes, the extensional modes, and the thickness-shear modes. The three out-of-plane mode types are the coupled twist-bending modes, the torsional modes, and the transverse thickness-shear modes.

In this study, the concept of multimodal vibration damping via an analogous electrical network will be enhanced to be able to attenuate both in-plane and out-of-plane vibration modes while also considering shear deformation and rotary inertia to be able to accurately model thick rings. While the enhanced electrical networks will be capable of replicating the thickness-shear modes for both out-of-plane and in-plane vibrations, this study opts to neglect these modes due to less practical applications at such high frequencies. Experimental investigations are not conducted due to the reliance on numerical simulations that provide sufficient insight into the behavior of rings. Furthermore, analogous network damping has already been validated for thin rings [29]. The present study serves as a theoretical foundation for future experimental implementation as the complexity of the electrical network makes it difficult to build a physical analog network. However, digital or synthetic networks may prove to be the solution when it comes to experimentally validating the network topology. Recent developments by Raze et al. [35] offers a modeling framework to digitize shunt and networks, eliminating the need for bulky magnetic circuit components in complex topologies. Furthermore, Zheng [36] has developed a piezoelectric meta-ring with digital shunting circuits in rings for programmable bandgaps.

In Section 2, the governing equations for the ring are derived for both in-plane and out-of-plane motions. In Section 3, the analogous electrical network for in-plane vibrations is developed. In Section 4, the analogous network for the out-of-plane vibrations is developed. In Section 5, the passive electrical components are tuned using frequency coherence conditions, and both in-plane and out-of-plane networks are numerically coupled to a thick ring to measure the frequency response function of the structure to a point force excitation.

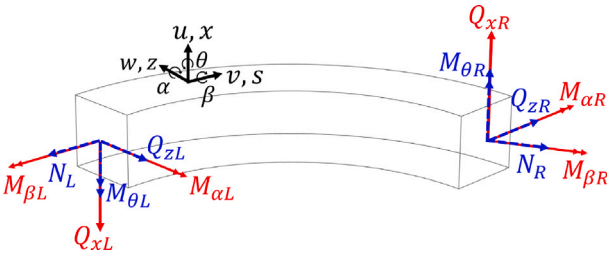

Fig. 1. Segment of a curved beam with internal forces and moments. In-plane components are marked as (·····), and out-of-plane components are marked as (——). Single headed arrows indicate forces while double headed arrows indicate moments.

2. Governing equations for the vibrations of a ring

2.1. Governing for in-plane vibrations

Consider a segment of a ring as shown in Fig. 1. The governing equations of motion for the in-plane vibrations of a segment of curved beam [9] of Young's Modulus E, Poisson ratio ν, cross sectional area A, and area moment of inertia I_x is given by

$$\begin{aligned} \frac{\partial N}{\partial s}+\frac{Q_z}{R}&=\rho A\frac{\partial^2 v}{\partial t^2}, & M_\theta &= EI_x\frac{\partial \theta}{\partial s},\\ \frac{\partial Q_z}{\partial s}-\frac{N}{R}&=\rho A\frac{\partial^2 w}{\partial t^2}, & N &= EA\left(\frac{\partial v}{\partial s}+\frac{w}{R}\right),\\ Q_z+\frac{\partial M_\theta}{\partial s}&=\rho I_x\frac{\partial^2 \theta}{\partial t^2}, & Q_z &= kAG\phi_i,\\ & & \phi_i+\theta &= \frac{\partial w}{\partial s}-\frac{v}{R}, \end{aligned} \tag{1}$$

where w is the radial displacement, v is the circumferential displacement, Q_z is the flexural shear force, M_θ is the bending moment, θ is the slope of the deflection curve when the shear force is neglected, and ϕ_i is the angle of shear along the neutral axis at the same cross section. The total deflection is the sum of both θ and ϕ_i. Note that when the angle of shear $\phi_i = 0$, the inertial term $I_x = 0$, and the radius $R \to \infty$, we recover the equations of motion for the Euler–Bernoulli beam equations. Furthermore, if we only consider that the radius $R \to \infty$, then we recover the equations of motion of a Timoshenko beam. The shear modulus is given as $G = E/(2(1+\nu))$. The constant k, which appears in the definition of Q_z, is the Timoshenko shear coefficient that accounts for the non-uniform strain along the cross-section of the beam. This value is typically taken to be $k = 5/6$ for rectangular sections, but other more complex and detailed formulations exist [37]. These in-plane equations of motion describe three types of vibration modes: inextensional bending modes, extensional bending modes, and thickness-shear modes. The first three mode shapes for each of the three mode types are shown in Fig. 2. The number of wavelengths for each mode is indicated by n.

Following Kirkhope's formulation [38], The natural frequencies of a free ring undergoing in-plane vibration can be determined by solving the dynamic stiffness matrix given as

$$\det\begin{pmatrix} a_{11} & a_{12} & a_{13}\\ a_{12} & a_{22} & a_{23}\\ a_{13} & a_{23} & a_{33}\end{pmatrix}=0$$

where

$$\begin{aligned} a_{11} &= \pi R\left[\left(\frac{EI_x}{R^4}(n^2-1)^2+\frac{EA}{R^2}\right)-\omega_n^2\left(\rho A+\frac{\rho I_x}{R^2}n^2\right)\right], & a_{22} &= \pi R\left[\left(\frac{EI_x}{R^2}n^2+kGA\right)-\omega_n^2\rho I_x\right],\\ a_{12} &= \pi R\left[\left(\frac{EI_x}{R^3}n(n^2-1)+\frac{EA}{R^2}\right)-\omega_n^2\left(\frac{\rho I_x}{R}n\right)\right], & a_{23} &= \pi R\left[\omega_n^2\frac{2\rho I_x}{R}\right],\\ a_{13} &= \pi R\left[\left(-\frac{EA}{R^2}n\right)-\omega_n^2\left(-\frac{2\rho I_x}{R^2}n\right)\right], & a_{33} &= \pi R\left[\left(\frac{EA}{R^2}n^2\right)-\omega_n^2\left(\rho A+\frac{3\rho I_x}{R^2}\right)\right]. \end{aligned} \tag{2}$$

Expansion of the determinant results in a cubic frequency equation that when solved returns three frequencies, ω_n^2 for each mode number n, corresponding to the in-plane inextensional mode as the lowest frequency, extensional mode as the middle frequency, and thickness-shear mode as the highest frequency. Inextensional bending modes are defined when $n \geq 2$ since there are no single wavelength bending modes for circular symmetric structures. Extensional modes and thickness-shear modes are defined when $n \geq 0$.

2.2. Governing equations for out-of-plane vibrations

Following Rao's [9] derivation of a curved beam undergoing out-of-plane vibrations, consider the free body diagram of a segment of curved beam shown in Fig. 1, where Q_x represents the transverse shear force along the transverse axis x, M_β represents the torsional moment about the tangential axis s, and M_α represents the bending moment about the radial axis z. The force equation of

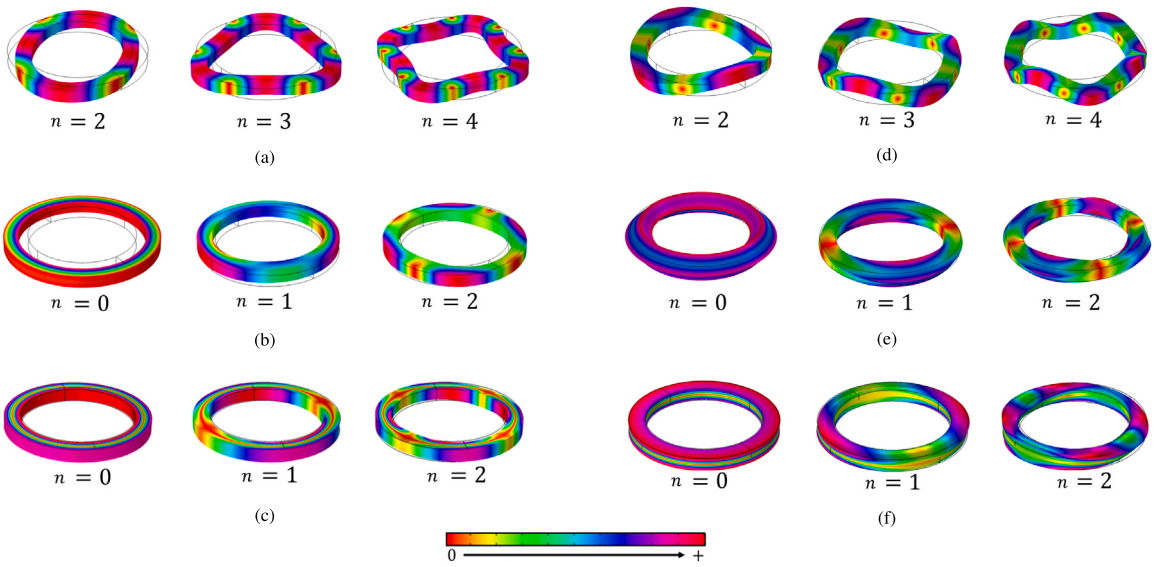

Fig. 2. Different types of vibration modes for a thick circular ring. In-plane mode shapes: (a) inextensional bending modes, (b) extensional modes, (c) thickness-shear modes. Out-of-plane mode shapes: (d) coupled twist-bending modes, (e) torsional modes, (f) transverse thickness-shear modes. In the numerical example, the rectangular cross section width to thickness ratio is $\frac{b}{h} = \frac{4}{5}$, and the thickness to radius ratio is $\frac{h}{R} = \frac{1}{4}$. The colors corresponds to the displacement magnitude, as indicated in the colorbar.

motion in the transverse direction and the two moment equations of motions in the radial and tangential direction for a thin curved ring of radius R, cross-sectional area of A, area moment of inertia I_z, and density ρ can be given as

$$\begin{aligned} \frac{\partial Q_x}{\partial s} &= \rho A \frac{\partial^2 u}{\partial t^2}, \\ \frac{\partial M_\alpha}{\partial s} + \frac{M_\beta}{R} - Q_x &= \rho I_z \frac{\partial^2 \alpha}{\partial t^2}, \\ \frac{\partial M_\beta}{\partial s} - \frac{M_\alpha}{R} &= \rho J_s \frac{\partial^2 \beta}{\partial t^2}, \end{aligned} \tag{3}$$

respectively, where u denotes the transverse displacement along the x axis. For rectangular cross-sections, the torsional constant is given by $J_s = Cbh^3$, where b denotes the longer side of the cross-section, h denotes the shorter side of the cross-section, and C is the torsional rigidity multiplier for a given geometry of the cross section [39]. Note that for a rectangular cross-section there are no exact close form solutions, but the torsional rigidity multiplier can be approximately estimated by looking up the aspect ratio in a table of experimentally determined values.

The bending moment along the radial axis and the torsional moment takes the form

$$\begin{aligned} M_\alpha &= EI_z \left(\frac{\beta}{R} - \frac{\partial \alpha}{\partial s} \right), & Q_x &= kAG\phi_o, \\ M_\beta &= GJ_s \left(\frac{\alpha}{R} + \frac{\partial \beta}{\partial s} \right), & \phi_o + \alpha &= \frac{\partial u}{\partial s}, \end{aligned} \tag{4}$$

where EI_z is the transverse flexural stiffness, GJ_s is the torsional stiffness, and kAG is the shear stiffness. The angular displacement of the cross section due to radial bending is given by α, β is the angular displacement of the cross section due to torsional displacement along the tangential axis, and ϕ_o is the angle of shear along the neutral axis at the same cross section. The total deflection is the sum of both α and ϕ_o. When the angle of shear $\phi_o = 0$, the equations of motion for the out-of-plane vibrations of a thin disk-like ring are recovered. These out-of-plane equations of motion describe three types of vibration modes: coupled twist-bending modes, torsional modes, and transverse thickness-shear modes. The first three mode shapes for each of the three mode types are shown in Fig. 2.

It is possible to isolate the governing equations to model purely torsional vibrations. The equations of motion that describe torsional vibrations can be determined from the equations for out-of-plane vibrations, as torsion is a subset of the out-of-plane vibrations. The torsion equations can be isolated when the transverse displacement u is small compared to the twist angular displacement β. As a result, all terms involving the transverse displacement u and the radial angular displacement α can be ignored leaving the equations of motion for pure torsional vibration as

$$\frac{\partial M_\beta}{\partial s} - \frac{M_\alpha}{R} = \rho J_s \frac{\partial^2 \beta}{\partial t^2}, \qquad M_\alpha = EI_z \frac{\beta}{R}, \qquad M_\beta = GJ_s \frac{\partial \beta}{\partial s}. \tag{5}$$

Following Rao's [9] formulation, the natural frequencies of a free ring undergoing out-of-plane vibration can be determined by solving the polynomial equation given as

$$\omega_n^6\left(\frac{\rho AR^4}{EI_z}\right)^3\frac{S_1S_2^3S_4S_5}{S_3}-\omega_n^4\left(\frac{\rho AR^4}{EI_z}\right)^2\left[n^4S_2^2\left(S_1S_4+\frac{S_5}{S_3}+\frac{S_1S_4S_5}{S_3}\right)+\frac{S_1S_2^2S_4}{S_3}+S_1S_2^2S_4S_5+\frac{S_2S_5}{S_3}\right]$$
$$+\omega_n^2\left(\frac{\rho AR^4}{EI_z}\right)\left[S_1S_2S_4+S_5+n^2\left(1+\frac{S_2}{S_3}-2S_1S_2S_4+S_2S_5\right)+n^4S_2\left(1+S_1S_4+\frac{S_5}{S_3}\right)\right]$$
$$+(-n^6+2n^4-n^2)=0 \tag{6}$$

where

$$S_1=\frac{E}{G},\qquad S_2=\frac{I_z}{AR^2},\qquad S_3=\frac{I_z}{J_s},\qquad S_4=\frac{1}{k},\qquad S_5=\frac{EI_z}{GJ_s}. \tag{7}$$

Solving this polynomial equation for the frequency, ω_n^2, returns three values for each n mode number: the twist-bending mode as the lowest frequency, the torsional mode as the middle frequency, and the transverse thickness shear mode as the highest frequency. Twist-bending modes are defined when $n \geq 2$ since there are no single wavelength bending modes for circular symmetric structures. Torsional modes and transverse thickness-shear modes are defined when $n \geq 0$.

3. Development of the analogous electrical networks to the in-plane vibrations of a ring

3.1. Finite difference scheme

A finite difference scheme is applied to the differential equations of motion to define a discrete model that will become the voltage and current equations of the electrical network. The choice in the discrete scheme is largely responsible for the simplification in the realizable networks [40]. The finite difference scheme used by Darleux [28] is used in this case to discretize the continuous equations for the curved beam.

3.2. Analogous discrete equations

By applying the finite difference scheme to Eqs. (1), the discretized set of mechanical equations can be given as

$$\begin{aligned}
-\frac{m}{2}\omega^2V_L&=N_I-N_L+\frac{a}{2R}Q_L,\\
-\frac{m}{2}\omega^2V_R&=N_R-N_I+\frac{a}{2R}Q_R,\\
-m\omega^2W_I&=Q_R-Q_L-\frac{a}{R}N_I,\\
-\frac{I}{2}\omega^2\theta_L&=\frac{a}{2}Q_L+M_I-M_L,\\
-\frac{I}{2}\omega^2\theta_R&=\frac{a}{2}Q_R+M_R-M_I,
\end{aligned}\qquad
\begin{aligned}
M_{\theta_I}&=K_\theta(\theta_R-\theta_L),\\
N_I&=K_v\left(V_R-V_L+\frac{a}{R}W_I\right),\\
Q_{z_L}&=\frac{K_w}{2}(W_I-W_L-\frac{a}{2R}V_L-\frac{a}{2}\theta_L),\\
Q_{z_R}&=\frac{K_w}{2}(W_R-W_I-\frac{a}{2R}V_R-\frac{a}{2}\theta_R),
\end{aligned} \tag{8}$$

where a refers to the length of the unit cell in the finite difference scheme. The variables W and V are the frequency domain counterparts of the time domain displacements w and v, respectively. The mass m replaces the term ρAa, rotary inertia I replaces the term $\rho I_x a$, K_v is the longitudinal stiffness replacing EA/a, K_θ is the bending stiffness replacing EI_x/a, and K_w is the shear stiffness replacing kAG/a.

Applying a direct electromechanical analogy to the equations of motion, which relates mass to inductance and the inverse of stiffness to capacitance, the discretized set of analogous electrical equations can be given as

$$\begin{aligned}
-\frac{L}{2}\omega^2q_{v_L}&=V_{v_L}-V_{v_I}-\frac{\hat{a}}{2\hat{R}}V_{w_L},\\
-\frac{L}{2}\omega^2q_{v_R}&=V_{v_I}-V_{v_R}-\frac{\hat{a}}{2\hat{R}}V_{w_R},\\
-L\omega^2q_{w_I}&=V_{w_L}-V_{w_R}-\frac{\hat{a}}{\hat{R}}V_{v_I},\\
-\frac{L_\theta}{2}\omega^2q_{\theta_L}&=\frac{\hat{a}}{2}V_{w_L}+V_{\theta_I}-V_{\theta_L},\\
-\frac{L_\theta}{2}\omega^2q_{\theta_L}&=\frac{\hat{a}}{2}V_{w_R}+V_{\theta_R}-V_{\theta_I},
\end{aligned}\qquad
\begin{aligned}
C_\theta V_{w_I}&=q_{\theta_L}-q_{\theta_R},\\
C_v V_{v_I}&=q_{v_L}-q_{v_R}-\frac{\hat{a}}{\hat{R}}q_{w_I},\\
C_w V_{w_L}&=q_{w_I}-q_{w_L}-\frac{\hat{a}}{2\hat{R}}q_{v_L}-\frac{\hat{a}}{2}q_{\theta_L},\\
C_w V_{w_R}&=q_{w_R}-q_{w_I}-\frac{\hat{a}}{2\hat{R}}q_{v_R}-\frac{\hat{a}}{2}q_{\theta_R},
\end{aligned} \tag{9}$$

where the inductance L is the electrical analogue of the mass of the unit cell, the inductance L_θ is the electrical analogue of the rotary inertia of the unit cell, the capacitance C_θ is the electrical analogue of the bending stiffness in the unit cell, C_v is the electrical analogue of the longitudinal stiffness in the unit cell, and C_w is the electrical analogue of the shear stiffness in the unit cell.

3.3. Spatial and frequency coherence conditions

To ensure that the electrical modes match the mechanical modes, spatial and frequency conditions must be met to determine the appropriate electrical constants. Spatial coherence refers to the resemblance between the physical shapes of mechanical modes and their corresponding electrical modes. This requires sufficient discretization to accurately represent the desired mode shapes, as well as accounting for the appropriate mechanical boundary conditions in the electrical domain. Then, if there are insufficient unit cells in the electrical network, the spatial modes may not show an accurate representation of the actual ring mode shape. Spatial coherence can be assured by adhering to the criteria previously described in [27] as

$$\frac{n_{element}}{N_{max}} \geq 10, \tag{10}$$

which says that the number of elements in the structure ($n_{element}$) has to be ten times or greater than the maximum number of wavelengths (N_{max}) in the frequency range.

In the present case, the structure is closed on itself, so there are no explicit boundary conditions that need to be defined. Frequency coherence ensures that the natural frequencies of the electrical network matches the natural frequencies of the discretized model of the mechanical ring which ensures similar wave propagation properties. Applying a strict electromechanical analogy between the two domains is not necessary or ideal as it constrains the degree of freedom in network tuning. Instead, the frequency coherence is derived by equating the mechanical and electrical transfer matrices, as shown by Darleux [28] for curved beams. The mechanical and electrical transfer matrices are determined by solving Eqs. (8) and (9) for all terms on the right of the unit cell. With the additional terms for shear deformation and rotary inertia, the mechanical and electrical transfer matrices for the in-plane motions can be defined by

$$\begin{pmatrix} W \\ \theta \\ V \\ Q_z \\ M_\theta \\ N \end{pmatrix}_R^* = \mathbf{T}^*_{\mathbf{M,IP}} \begin{pmatrix} W \\ \theta \\ V \\ Q_z \\ M_\theta \\ N \end{pmatrix}_L^* , \quad \begin{pmatrix} q_w \\ q_\theta \\ q_v \\ V_w \\ V_\theta \\ V_v \end{pmatrix}_R^* = \mathbf{T}^*_{\mathbf{E,IP}} \begin{pmatrix} q_w \\ q_\theta \\ q_v \\ V_w \\ V_\theta \\ V_v \end{pmatrix}_L^* \tag{11}$$

where $\mathbf{T}^*_{\mathbf{M,IP}}$ is defined by Eq. (A.1) and the superscript, *, indicates nondimensionalized quantities. Then, equating each constant in the mechanical transfer matrix to the equivalent constant in the electrical transfer matrix, the frequency coherence of the in-plane vibration of a curved beam element, the conditions are given as

$$\begin{aligned} &\frac{a}{R} = \frac{\hat{a}}{\hat{R}}, \quad && \frac{K_v}{m} = \frac{1}{LC_v}, \quad && \frac{K_\theta}{a^2 m} = \frac{1}{\hat{a}^2 LC_\theta}. \\ &\frac{K_\theta}{I} = \frac{1}{L_\theta C_\theta}, && \frac{K_w}{m} = \frac{1}{LC_w}, \end{aligned} \tag{12}$$

3.4. Network development and eigenvalue analysis

The discretized electrical equations are developed into the electrical network shown in Fig. 3. The single unit cell consists of 5 inductors, 4 capacitors, and 5 transformers; however, for simplification purposes, edge components may be combined [32] reducing the count to 3 inductors, 3 capacitors, and 3 transformers. Consider a thick ring with an outer radius of 225 mm, inner radius of 175 mm, and depth of 40 mm. To verify the convergence of the network to this ring, an eigenvalue analysis is performed on an electrical network consisting of 100 unit cells. The eigenvalues are shown in Table 1 with the corresponding finite element method (FEM) ring natural frequencies for comparison. The FEM ring is adequately meshed to ensure convergence of the natural frequencies. It can be observed for the inextensional bending modes that the error increases as the mode number increases, due to insufficient discretization of the electrical network. For the extensional and thickness-shear modes, the error does not scale as consistently with mode number due to more empirical constants used in the model.

4. Development of the analogous electrical networks to the out-of-plane vibrations of a ring

4.1. Analogous discrete equations

By applying a finite difference scheme to Eqs. (3) and (4), the discretized set of mechanical equations can be given as

$$\begin{aligned} -m\omega^2 U_I &= Q_{x_R} - Q_{x_L}, \\ -\frac{I_\alpha}{2}\omega^2 \alpha_L &= M_{\alpha_I} - M_{\alpha_L} + \frac{a}{2R} M_{\beta_L} - \frac{a}{2} Q_{x_L}, \\ -\frac{I_\alpha}{2}\omega^2 \alpha_R &= M_{\alpha_R} - M_{\alpha_I} + \frac{a}{2R} M_{\beta_R} - \frac{a}{2} Q_{x_R}, \\ -I_\beta \omega^2 \beta_I &= M_{\beta_R} - M_{\beta_L} - \frac{a}{R} M_{\alpha_I}, \end{aligned} \qquad \begin{aligned} M_{\alpha_I} &= K_\alpha \left(\frac{a}{R}\beta_I - \alpha_R + \alpha_L \right), \\ M_{\beta_L} &= \frac{K_\beta}{2} \left(\frac{a}{2R}\alpha_L + \beta_I - \beta_L \right), \\ M_{\beta_R} &= \frac{K_\beta}{2} \left(\frac{a}{2R}\alpha_R + \beta_R - \beta_I \right), \\ Q_L &= \frac{K_u}{2}(U_I - U_L - \frac{a}{2}\alpha_L), \\ Q_R &= \frac{K_u}{2}(U_R - U_I - \frac{a}{2}\alpha_R), \end{aligned} \tag{13}$$

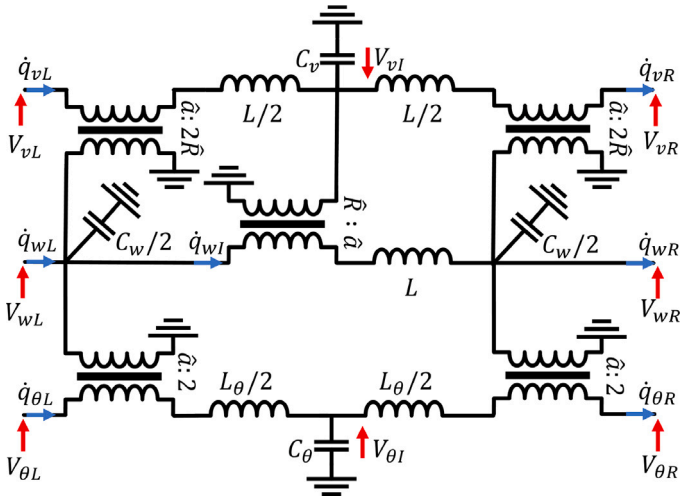

Fig. 3. Electrical network analogous to in-plane vibrations of rings.

Table 1
Natural frequencies of the in-plane ring electrical network with 100 unit cells compared to analytical frequencies and FEM frequencies. The percent error to the FEM frequencies for the analytical and network values are in parentheses.

Mode	FEM	Analytical	Network
Inextensional modes (Hz)			
2	757.16	752.81 (0.57%)	744.73 (1.64%)
3	2049.49	2034.19 (0.75%)	2007.12 (2.07%)
4	3718.36	3684.27 (0.92%)	3628.85 (2.41%)
5	5654.23	5593.05 (1.08%)	5499.44 (2.74%)
6	7776.21	7679.95 (1.24%)	7536.87 (3.08%)
Extensional modes (Hz)			
0	4064.40	4033.30 (0.77%)	4019.94 (1.09%)
1	5634.13	5628.75 (0.10%)	5669.68 (0.63%)
2	8834.67	8849.59 (0.17%)	8969.14 (1.52%)
Thickness-shear modes (Hz)			
0	31 364	31524 (0.51%)	31258 (0.34%)
1	31 695	31878 (0.58%)	31599 (0.30%)
2	32 650	32903 (0.77%)	32582 (1.52%)

where m represents the mass of the element and replaces the quantity ρAa, I_α represents the rotary inertia term, I_β represents the polar inertia term, K_α is the transverse bending stiffness replacing EI_z/a, K_β is the torsional stiffness replacing GJ_s/a, and K_u is the shear stiffness replacing kAG/a.

Applying the direct electromechanical analogy to the discrete mechanical equations results in the following electrical equations that describe out-of-plane ring vibrations:

$$
\begin{aligned}
-L_u\omega^2 q_{u_I} &= V_{u_L} - V_{u_R}, \\
-\frac{L_\alpha}{2}\omega^2 q_{\alpha_L} &= V_{\alpha_L} - V_{\alpha_I} - \frac{\hat{a}}{2\hat{R}}V_{\beta_L} - \frac{\hat{a}}{2}V_{u_L}, \\
-\frac{L_\alpha}{2}\omega^2 q_{\alpha_R} &= V_{\alpha_I} - V_{\alpha_R} - \frac{\hat{a}}{2\hat{R}}V_{\beta_R} - \frac{\hat{a}}{2}V_{u_R}, \\
-L_\beta\omega^2 q_{\beta_I} &= V_{\beta_L} - V_{\beta_R} - \frac{\hat{a}}{\hat{R}}V_{\alpha_I},
\end{aligned}
\qquad
\begin{aligned}
C_\alpha V_{\alpha_I} &= -\frac{\hat{a}}{\hat{R}}q_{\beta_I} - q_{\alpha_R} + q_{\alpha_L}, \\
C_\beta V_{\beta_L} &= \frac{\hat{a}}{2\hat{R}}q_{\alpha_L} + q_{\beta_I} - q_{\beta_L}, \\
C_\beta V_{\beta_R} &= \frac{\hat{a}}{2\hat{R}}q_{\alpha_R} + q_{\beta_R} - q_{\beta_I}, \\
C_u V_{u_L} &= q_{u_L} - q_{u_I} - \frac{\hat{a}}{2}q_{\alpha_L}, \\
C_u V_{u_R} &= q_{u_I} - q_{u_R} - \frac{\hat{a}}{2}q_{\alpha_R},
\end{aligned}
\tag{14}
$$

where the inductance L_u is the electrical analogue of the mass of the unit cell, the inductance L_α is the electrical analogue of the rotary inertia of the unit cell, the inductance L_β is the electrical analogue of the polar rotary inertia of the unit cell, the capacitance C_α is the electrical analogue of the transverse bending stiffness in the unit cell, C_β is the electrical analogue of the torsional stiffness in the unit cell, and C_u is the electrical analogue of the shear stiffness in the unit cell.

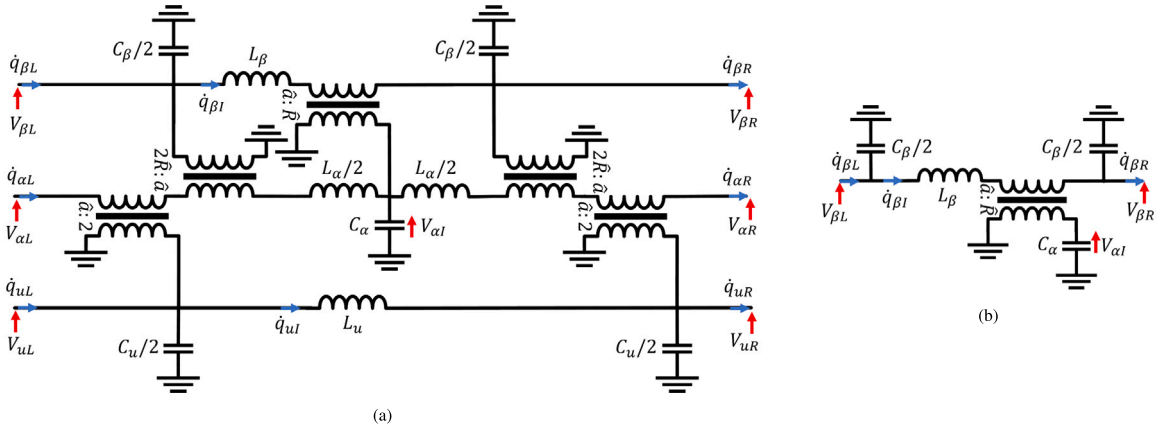

Fig. 4. Electrical networks analogous to (a) out-of-plane vibrations of rings and (b) special case for torsional vibrations of rings.

4.2. Frequency coherence conditions

The mechanical and electrical transfer matrices for the out-of-plane motions can be defined by

$$\begin{pmatrix} U \\ \alpha \\ \beta \\ M_\alpha \\ M_\beta \\ Q_x \end{pmatrix}_R^* = \mathbf{T}^*_{\mathbf{M,OP}} \begin{pmatrix} U \\ \alpha \\ \beta \\ M_\alpha \\ M_\beta \\ Q_x \end{pmatrix}_L^* , \quad \begin{pmatrix} q_u \\ q_\alpha \\ q_\beta \\ V_\alpha \\ V_\beta \\ V_u \end{pmatrix}_R^* = \mathbf{T}^*_{\mathbf{E,OP}} \begin{pmatrix} q_u \\ q_\alpha \\ q_\beta \\ V_\alpha \\ V_\beta \\ V_u \end{pmatrix}_L^* \tag{15}$$

where $\mathbf{T}^*_{\mathbf{M,OP}}$ is defined by Eq. (A.2).

By equating the terms in the mechanical transfer matrix and the electrical transfer matrix, the frequency coherence of the out-of-plane vibration of a curved beam element, the conditions are given as

$$\begin{aligned} &\frac{a}{R} = \frac{\hat{a}}{\hat{R}}, \quad && \frac{K_\beta}{I_\beta} = \frac{1}{L_\beta C_\beta}, \quad && \frac{K_\alpha}{I_\alpha} = \frac{1}{L_\alpha C_\alpha}, \\ &\frac{K_\alpha}{a^2 m} = \frac{1}{\hat{a}^2 L_u C_\alpha}, \quad && \frac{K_\alpha}{I_\beta} = \frac{1}{L_\beta C_\alpha}, \quad && \frac{K_u}{m} = \frac{1}{L_u C_u}. \end{aligned} \tag{16}$$

4.3. Network development and eigenvalue analysis

The discretized electrical equations are developed into the electrical network shown in Fig. 4(a) for the coupled twist-bending modes. The single unit cell consists of 4 inductors, 5 capacitors, and 5 transformers. By combining edge components, the simplified unit cell reduces to 3 inductors, 3 transformers, and 3 capacitors. It is also noted that for applications on purely torsional vibrations, further simplifications may be applied. The isolated network that represents the torsional modes is shown in Fig. 4(b).

For the same thick ring, an eigenvalue analysis is performed on an electrical network consisting of 100 unit cells. The eigenvalues are shown in Table 2. It is observed for the twist-bending modes that the percent error decreases up to the eighth mode, where after, the error will begin to increase again. This is also documented in literature of out-of-plane dynamics of rings, and the effects are emphasized for thicker cross sections and shorter radii [11]. This phenomenon can be attributed to the chosen dimensions of the ring approaching the boundaries where the dynamics of annular plates [41] become more significant and non-negligible. Indeed, as shown by Kirhope [10], using the annular plate equations to calculate the out-of-plane natural frequencies of thick rings resulted in improved convergence. We can confirm that the natural frequencies of the network are closer to the natural frequencies of the analytical model, which is based off ring dynamics, whereas the FEM frequencies take into account the effects of annular plates. As a result, it will be necessary to numerically optimize some of the electrical parameters [29] in order to improve the frequency coherence between network and structure.

5. Frequency response analysis of the coupled piezoelectric ring and electrical networks

5.1. Coupled system frequency response

The frequency response analysis of the coupled piezoelectric ring and electrical networks is simulated on the same ring of outer radius 225 mm, inner radius 175 mm, and depth 40 mm. Mechanical damping is prescribed in the structural model as frequency

Table 2
Natural frequencies of the out-of-plane ring electrical network with 100 unit cells compared to analytical frequencies and FEM frequencies. The percent error to the FEM frequencies for the analytical and network values are in parentheses.

Mode	FEM	Analytical	Network
Twist-bending modes (Hz)			
2	583.10	603.93 (3.57%)	602.53 (3.33%)
3	1615.03	1658.48 (2.69%)	1652.60 (2.33%)
4	2989.74	3057.96 (2.28%)	3041.32 (1.73%)
5	4630.61	4725.65 (2.05%)	4688.75 (1.26%)
6	6474.23	6598.25 (1.92%)	6528.55 (0.84%)
Torsional modes (Hz)			
0	2525.99	2528.51 (0.10%)	2534.15 (0.32%)
1	3387.57	3510.83 (3.64%)	3514.56 (3.75%)
2	5199.95	5512.53 (6.01%)	5512.17 (6.00%)
Thickness-shear modes (Hz)			
0	38745	39197 (1.17%)	39196 (1.16%)
1	38910	39469 (1.44%)	39469 (1.44%)
2	39349	40266 (2.33%)	40265 (2.33%)

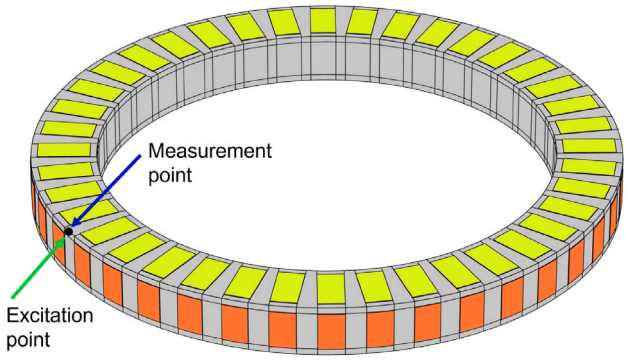

Fig. 5. Thick ring with a set of 40 patches for controlling in-plane modes (placed on the external cylindrical surface of the ring) and a set of 40 patches for controlling out-of-plane modes (placed on the top plane surface of the ring).

dependent isotropic loss factor following experimental data for 6061 aluminum [42]. The mesh size used in the finite element model to ensure convergence of the natural frequencies is 6 mm, which is approximately 2% of the size of the shortest wavelength involved in the study.

In the numerical simulation, we consider 40 unit cells for both the in-plane and out-of-plane modes. The out-of-plane electrical network is coupled to the flat side of the ring using 40 PIC255 patches with dimensions of 20 mm by 40 mm, which serve as the C_α capacitance. The in-plane electrical network is coupled to the curved side of the ring using 40 piezoelectric patches with dimensions 20 mm by 30 mm. These patches serve as the C_θ capacitance. With 40 patches, according to spatial coherence criteria shown in Eq. (10), it should be possible to optimally tune to the fourth wavelength mode (third bending mode) for both in-plane and out-of-plane vibrations. The 3D model of the piezoelectric ring is shown in Fig. 5. In all, the piezoelectric patches only add approximately 2.25% additional mass to the structure.

The capacitance value of the piezoelectric patch was calculated by applying a 1 V frequency swept input voltage and integrating the surface charge along the top surface of the patch for each set of patches controlling in-plane and out-of-plane modes. The capacitance is equivalent to the value of surface charge due to the unit voltage input. Since the capacitance is frequency dependent, an average value is taken in between resonances. Using these capacitance values, C_θ for in-plane and C_α for out-of-plane, the other electrical constants such as the inductance and the transformer ratios are derived from the frequency coherence conditions in Eqs. (12) and (16).

To address the unaccounted dynamics of the annular plate in the model, we conducted supplementary numerical optimization, where the objective function is specifically aimed at minimizing errors in the first three bending modes and the first torsional mode. The L_β and L_u inductors of the out-of-plane network are adjusted in the optimization process. Compared to the initial values derived from the frequency coherence conditions, the optimized L_β inductor differs by 4.73% and the optimized L_u inductor differs by 4.58%.

Table 3
Values of components used in the electrical unit cell.

Network type	Component	Value
In-plane	Capacitor (C_θ)	11.45 nF
In-plane	Capacitor (C_v)	39.50 nF
In-plane	Capacitor (C_w)	41.00 nF
In-plane	Inductor (L)	0.972 mH
In-plane	Inductor (L_θ)	1.758 mH
In-plane	Resistor (R_{IP})	70 Ω
In-plane	Resistor (R_{Ext})	0.75 Ω
Out-of-plane	Capacitor (C_α)	15.15 nF
Out-of-plane	Capacitor (C_β)	7.917 nF
Out-of-plane	Capacitor (C_u)	21.00 nF
Out-of-plane	Inductor (L_u)	1.255 mH
Out-of-plane	Inductor (L_α)	1.312 mH
Out-of-plane	Inductor (L_β)	6.598 mH
Out-of-plane	Resistor (R_{TB})	46 Ω
Out-of-plane	Resistor (R_{Tor})	7 Ω
Both	Transformer ($\hat{a} : \hat{R}$)	0.1571
Both	Transformer ($\hat{a} : 1$)	4

The optimal resistance per unit cell can be calculated according to Porfiri [22] and Lossouarn et al. [43] for simply supported beams following the formulation

$$R = k_c \hat{a} \sqrt{2L/C}. \tag{17}$$

Although there are no analytical equations for the optimal resistances in circular rings, this formulation serves as a baseline approximation for the optimal resistance in a unit cell where the inductance, capacitance, and transformer ratio are modified depending on the specific network and mode to be damped. The resistor, R_{IP}, is placed in series with the $\hat{a} : 2$ transformer in the in-plane network. Using the coupling factor of the first in-plane bending mode, the optimal resistance can be calculated by

$$R_{IP} = k_{c,IP} \frac{\hat{a}}{2} \sqrt{\frac{2L}{C_\theta}}. \tag{18}$$

The resistor for damping extensional modes, R_{Ext}, is placed in series with the C_v capacitor, and can be approximated by the expression

$$R_{Ext} = k_{c,IP} \frac{\hat{a}}{2} \sqrt{\frac{2L}{C_v}}. \tag{19}$$

The resistor, R_{TB}, is placed in series with the $\hat{a} : 2$ transformer in the out-of-plane network. Using the coupling factor of the first out-of-plane twist-bending mode, the optimal resistance can be calculated by

$$R_{TB} = k_{c,OP} \frac{\hat{a}}{2} \sqrt{\frac{2L_u}{C_\alpha}}. \tag{20}$$

The resistor, R_{Tor}, is placed in series with the $\hat{a} : \hat{R}$ transformer in the out-of-plane network, which damps the torsional modes. Using the coupling factor of the first out-of-plane torsional mode, the resistance can be approximated by

$$R_{Tor} = k_{c,OP} \frac{\hat{a}}{\hat{R}} \sqrt{\frac{2L_\beta}{C_\beta}}. \tag{21}$$

The values of the electrical components are shown in Table 3.

The comparison of the electrical eigenvalues to the mechanical eigenvalues of the ring is shown in Table 4. The mode types are labeled as: out-of-plane coupled twist-bending modes (TB), in-plane inextensional bending modes (IB), out-of-plane torsional modes (Tor), and one in-plane extensional mode (Ext). The number following each label corresponds to the number of wavelengths of that mode.

The electromechanical coupling factors of the piezoelectric patches are calculated separately for each network. The coupling factors for the patches controlling in-plane vibrations and patches controlling out-of-plane vibrations are given by

$$k_{c,IP} = \sqrt{\frac{\omega_{OC,IP}^2 - \omega_{SC}^2}{\omega_{SC}^2}}, \qquad k_{c,OP} = \sqrt{\frac{\omega_{OC,OP}^2 - \omega_{SC}^2}{\omega_{SC}^2}}, \tag{22}$$

respectively, where $\omega_{OC,IP}$ is the open circuit frequency for the in-plane patches when the out-of-plane patches are shorted, $\omega_{OC,OP}$ is the open circuit frequency for the out-of-plane patches when the in-plane patches are shorted, and ω_{SC} is the short circuit frequency of the piezoelectric ring when the patches of both networks are shorted. The electromechanical coupling factors of the ring are

Table 4
Natural frequencies of both in-plane and out-of-plane electrical networks with 40 unit cells compared to the FEM natural frequencies. The percent error to the FEM frequencies are in parentheses.

Mode	FEM (Hz)	Network (Hz)
TB2	582.17	582.38 (0.04%)
IB2	756.10	755.65 (0.05%)
TB3	1610.54	1603.61 (0.43%)
IB3	2046.13	2041.24 (0.24%)
Tor0	2500.88	2500.51 (0.01%)
TB4	2979.30	2964.68 (0.49%)
Tor1	3356.93	3495.67 (4.13%)
IB4	3710.85	3693.43 (0.47%)
Ext0	4030.32	4034.68 (0.11%)

Table 5
Electromechanical coupling factors for the natural frequencies of a thick ring. The values that are considered for the respective networks are in bold.

Mode	Coupling factors	
	In-plane $k_{c,IP}$	Out-of-plane $k_{c,OP}$
TB2	1.58%	**5.69%**
IB2	**4.57%**	2.99%
TB3	1.65%	**6.00%**
IB3	**4.43%**	2.88%
Tor0	1.83%	**6.86%**
TB4	1.64%	**6.02%**
Tor1	1.34%	**5.18%**
IB4	**4.31%**	2.74%
Ext0	**2.62%**	3.81%

Table 6
Effective electromechanical coupling factors for the natural frequencies of a thick ring. The values that are considered for the respective networks are in bold.

Mode	Effective coupling factors	
	In-plane $k_{c,IP}$	Out-of-plane $k_{c,OP}$
TB2	0.30%	**4.17%**
IB2	**4.16%**	1.10%
TB3	0.23%	**5.07%**
IB3	**4.06%**	1.95%
Tor0	0.05%	**5.14%**
TB4	0.35%	**5.19%**
Tor1	0.23%	**3.17%**
IB4	**3.97%**	0.39%
Ext0	**0.43%**	3.29%

shown in Table 5. Note that each mode exists in pairs for circular structures, so for each mode of the same wavelength, there are two separate but identical coupling factors.

With complex electrical network involving capacitors, the effective coupling factor is usually lower than what is calculated from Eq. (22). Following a method used by Lossouarn [43], we can calculate the effective coupling factors by computing two characteristic frequencies. The first frequency is determined by setting all the inductors in the network towards a very high inductance. The second frequency is determined by setting all the inductors in the network towards 0 H. Then, we can proceed with the calculation of the effective coupling factors as the traditional method. The effective coupling factors are shown in Table 6. Noticeably, the coupling factors are lower than the ones shown in Table 5, especially the Ext0 mode. This phenomenon can be explained by the using capacitance C_θ as the piezoelectric element, which, in practice, do not influence the extensional modes as strongly, as the direct analog to these modes lies in the capacitors C_v. Consequently, a single analogous network may not have the capability to effectively address all different modes by utilizing the same coupling capacitance.

The frequency response of the coupled structure is shown in Fig. 6. We observe significant multimodal damping across the frequency spectrum for different types of modes. However, it is noted that for the extensional mode, the damping performance is weak, which is attributed to poor coupling between the piezoelectric network and the structure, as shown in Table 6. We can see that Ext0 has higher coupling with the out-of-plane patches than the in-plane patches. In fact, the Ext0 mode is a type of breathing mode of the ring, where there is elongation rather than bending in the structure.

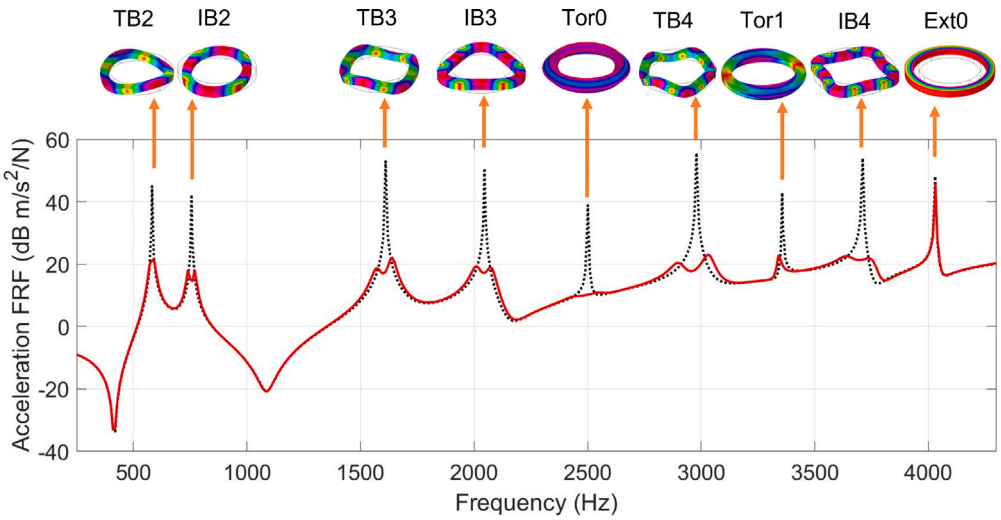

Fig. 6. Frequency response function of a thick ring with a set of 40 in-plane piezoelectric patches for damping in-plane modes and a set of 40 out-of-plane piezoelectric patches for damping out-of-plane modes coupled to their respective analogous networks (——) and the open-circuit response (– – –). Four types of modes are shown in this frequency response: Out-of-plane coupled twist-bending modes (TB), in-plane inextensional bending modes (IB), out-of-plane torsional modes (Tor), and one in-plane extensional mode (Ext). The number following each label corresponds to the number of wavelengths of that mode.

Table 7
Summary of the total vibration damping of each mode and associated effective coupling factor. Ext0* indicates the damping of the extensional mode from the results in Fig. 8.

Mode Type	Coupling Factor	Vibration Reduction (dB)
TB2	4.90%	23.53
IB2	4.08%	24.19
TB3	5.15%	30.85
IB3	3.96%	31.39
Tor0	5.88%	28.60
TB4	5.16%	32.61
Tor1	3.23%	20.15
IB4	3.92%	30.79
Ext0	0.10%	2.39
Ext0*	2.44%	23.49

The frequency response of the coupled system to the analogous torsional network shown in Fig. 4(b), is depicted in Fig. 7. The torsional network offers a simplified solution to the complex topology of the complete out-of-plane ring network. As anticipated, the network effectively attenuates the torsional modes within the structure. This selective damping is advantageous when it is only necessary to minimize damping in torsional modes, thereby simplifying the electrical network.

If the objective is to dampen the extensional modes, it is advisable to switch to using the C_v capacitor as the coupling element. Recall that the C_v capacitor is the electrical analogy to the extensional equations of the ring. We can recalculate the electrical parameters of the network following the frequency coherence parameters in Eq. (12). The electrical parameters for the in-plane network when coupled via the extensional C_v capacitor are shown in Table 8. The effective coupling factor for this network configuration is improved from 0.43% (C_θ coupling) to 2.44% (C_v coupling). The frequency response in Fig. 8 shows that the improved coupling leads to stronger damping effects. In Table 7, we observe a qualitative correlation between the coupling factor and the total attenuation. Modes with higher coupling factors show higher attenuation. Notably, for extensional modes, we observe improved coupling and vibration reduction when the in-plane network is coupled via the C_v capacitor rather than the C_θ capacitor.

6. Conclusion

This study has addressed the limitations of previous electrical network for vibration attenuation in rings and has introduced an enhanced approach capable of effectively damping vibrations in thick rings. By considering the influence of shear deformation and rotary inertia for both in-plane and out-of-plane vibrations, the proposed networks offers a comprehensive solution for multimodal vibration control in three-dimensional space. By coupling two separate analogous electrical networks derived from the respective

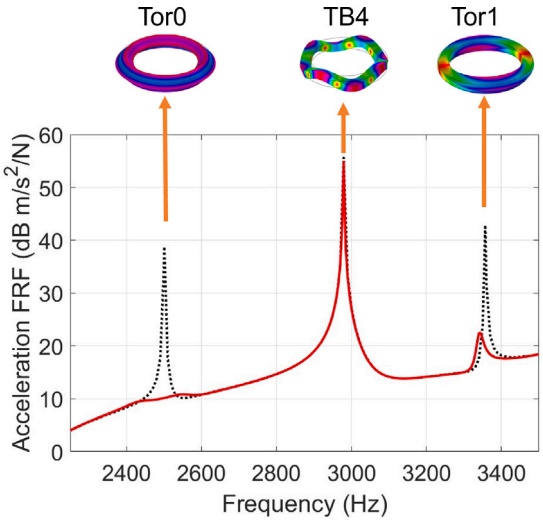

Fig. 7. Frequency response function of a thick ring with a set of 40 out-of-plane piezoelectric patches coupled to the analogous torsional network (——) and the open-circuit response (– – –).

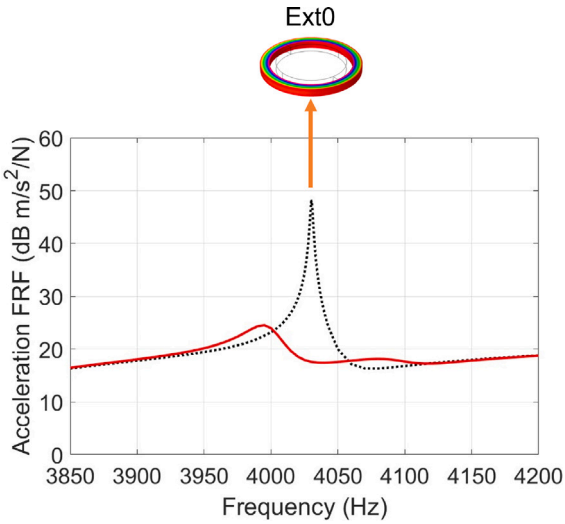

Fig. 8. Frequency response function of a thick ring coupled via the C_v capacitor to an analogous in-plane network (——) showing improved damping of the extensional mode, and the open-circuit response (– – –).

Table 8
Values of components used in the electrical unit cell of the in-plane network when coupled via the extensional C_v capacitor.

Network	Component	Value
In-plane	Capacitor (C_v)	11.45 nF
In-plane	Capacitor (C_θ)	3.405 nF
In-plane	Capacitor (C_w)	18.35 nF
In-plane	Inductor (L)	3.315 mH
In-plane	Inductor (L_θ)	5.700 mH
In-plane	Resistor (R_{IP})	70 Ω
In-plane	Resistor (R_{Ext})	70 Ω
In-plane	Transformer ($\hat{a}$: $\hat{R}$)	0.1571
In-plane	Transformer ($\hat{a}$: 1)	4

equations of motion, the proposed method replicates the dynamic behavior of thick rings and successfully mitigates vibrations for in-plane bending modes, out-of-plane twist-bending modes, and out-of-plane torsion. A simplified network has also been developed, enabling the selective targeting of torsion modes as needed, and it has proven highly effective in damping these specific modes. Furthermore, coupling the network to the structure via the C_v capacitor has introduced a method to damp the extensional modes.

In the presented numerical example, a substantial reduction in vibration exceeding 20 dB was observed across the entire spectrum, with the exception of the extensional mode where poor attenuation was attributed to suboptimal electromechanical coupling via the C_θ capacitor. However, when coupled via the C_v capacitor, the vibration reduction is significantly improved. Additionally, while analogously replicating shear modes through the electrical network is conceivable, the current example did not manifest this phenomenon due to coupling constraints and contextual relevance. It is noteworthy that the employed piezoelectric patch and network configuration (C_θ coupling) exhibited limited coupling with shear modes, which primarily occur at notably higher frequencies, rendering them less practically viable for vibration control within this specific study. Nonetheless, the results underscore the potential feasibility of emulating these shear modes if deemed necessary for future applications. Following the same method as damping extensional modes, it may be possible to damp the thickness-shear modes by coupling via the C_w or C_u capacitors.

Future research may focus on experimental validation of the proposed approach and further optimization to achieve even more efficient vibration damping in thick rings. By converting the analogous network to a digital model following the framework set by Raze et al. [35] the need for bulky magnetic circuit components in complex topologies can be eliminated and it would be more practical to conduct experiments to validate these numerical findings. Ultimately, this study contributes to the development of robust and reliable methods for multimodal vibration control, enhancing the performance and durability of structures incorporating thick rings.

CRediT authorship contribution statement

Alan Luo: Writing – review & editing, Writing – original draft, Visualization, Validation, Software, Methodology, Investigation, Formal analysis, Data curation, Conceptualization. **Boris Lossouarn:** Writing – review & editing, Supervision, Resources, Methodology, Conceptualization. **Alper Erturk:** Writing – review & editing, Supervision, Resources.

Declaration of competing interest

The authors declare that they have no known competing financial interests or personal relationships that could have appeared to influence the work reported in this paper.

Data availability

Data will be made available on request.

Appendix. Definition of transfer matrices

The mechanical transfer matrices are determined by solving the discrete mechanical equations for all of the terms on the right of the unit cell. Solving the set of discrete equations shown in Eq. (8) to be in the form shown in Eq. (11), the mechanical transfer matrix for the in-plane dynamics of a thick ring is given by

$$\mathbf{T}^*_{\mathbf{M,IP}} = \begin{bmatrix} A_{11} & A_{12} & A_{13} & A_{14} & \frac{1}{2} & \frac{\delta}{2} \\ 0 & A_{22} & 0 & -\frac{1}{2} & 1 & 0 \\ -\delta & -\frac{\delta}{2} & A_{33} & A_{34} & 0 & 1 \\ -\gamma & -\frac{\gamma}{2} & -\frac{\delta\gamma}{2} & A_{44} & 0 & 0 \\ \frac{\gamma}{2} & A_{52} & \frac{\delta\gamma}{4} & A_{54} & A_{55} & 0 \\ \delta\xi & \frac{\delta\xi}{2} & A_{63} & A_{64} & 0 & 1 \end{bmatrix} \tag{A.1}$$

where $A_{11} = 1 - 2\chi - \frac{\delta^2}{2}$, $A_{12} = -\frac{\mu}{4} - \frac{\delta^2}{4} - \chi$, $A_{13} = \delta - \frac{\delta^3}{4} - \delta\chi - \frac{\delta\xi}{4}$, $A_{14} = \frac{4\chi - 4\chi^2 - \delta^2\chi - \delta^2\xi}{\gamma} - \frac{1}{4}$, $A_{22} = -\frac{\mu}{2} - 1$, $A_{33} = 1 - \frac{\xi}{2} - \frac{\delta^2}{2}$, $A_{34} = -\frac{2\delta\chi}{\gamma} - \frac{\xi\delta}{2\gamma}$, $A_{44} = 1 - 2\chi$, $A_{52} = \frac{\mu^2}{4} + \frac{\gamma}{4}$, $A_{54} = \frac{\mu}{4} + \chi - 1$, $A_{55} = 1 - \frac{\mu}{2}$, $A_{63} = \frac{\delta^2\xi}{2} - \xi$, $A_{64} = -\frac{\delta\xi}{\gamma} + \frac{2\delta\xi\chi}{\gamma}$. The constants are defined as $\delta = \frac{a}{R}$, $\gamma = \frac{ma^2\omega^2}{K_\theta}$, $\mu = \frac{I\omega^2}{K_\theta}$, $\xi = \frac{m\omega^2}{K_v}$ and $\chi = \frac{m\omega^2}{K_w}$.

Similarly, solving the set of discrete equations shown in Eq. (13) to be in the form shown in Eq. (15), the mechanical transfer matrix for the out-of-plane dynamics of a thick ring is given by

$$\mathbf{T}^*_{\mathbf{M,OP}} = \begin{bmatrix} B_{11} & B_{12} & \frac{\delta}{2} & B_{14} & 0 & \delta \\ 0 & \frac{\delta^2}{2} & \delta & 0 & 0 & 2\delta \\ 0 & B_{32} & B_{33} & 0 & 0 & B_{36} \\ -\gamma & -\frac{\gamma}{2} & 0 & B_{44} & 0 & 0 \\ -\frac{\gamma}{2} & B_{52} & B_{53} & B_{54} & 1 & B_{56} \\ 0 & \frac{\delta\xi}{2} & -\xi & 0 & 0 & B_{66} \end{bmatrix} \tag{A.2}$$

where $B_{11} = 1 - 2\chi$, $B_{12} = 1 - \chi - \frac{\delta^2}{4}$, $B_{14} = \frac{4\chi}{\gamma} - \frac{4\chi^2}{\gamma}$, $B_{32} = \frac{\delta^3}{4} - \delta + \frac{\delta^2}{2}$, $B_{33} = 1 - \frac{\delta^2}{2} - 2\xi$, $B_{36} = 4 - 4\xi - \delta^2$, $B_{44} = 1 - 2\chi$, $B_{52} = \mu - \frac{\gamma}{4} - \frac{\delta^2\zeta}{4} - \frac{\delta^2\mu}{4}$, $B_{53} = \frac{\delta\zeta}{2} + \frac{\delta\mu}{2}$, $B_{54} = 1 - \chi$, $B_{56} = \delta\zeta + \delta\mu - \frac{\delta\zeta}{\xi}$, $B_{66} = 1 - 2\xi$. The constants are defined as $\delta = \frac{a}{R}$, $\gamma = \frac{ma^2\omega^2}{K_\alpha}$, $\mu = \frac{I_\alpha\omega^2}{K_\alpha}$ $\xi = \frac{I_\beta\omega^2}{K_\beta}$, $\zeta = \frac{I_\beta\omega^2}{K_\alpha}$ and $\chi = \frac{m\omega^2}{K_u}$. An electromechanical analogy is then used to convert mechanical terms into electrical terms, and the various ratios can be identified and used as frequency coherence conditions.

References

[1] S. Doshi, A. Katoch, A. Suresh, F.A. Razak, S. Datta, S. Madhavan, C.M. Zanhar, E. Gundabattini, A review on vibrations in various turbomachines such as fans, compressors, turbines and pumps, J. Vib. Eng. Technol. 9 (7) (2021) 1557–1575.
[2] T. Lu, A. Tsouvalas, A. Metrikine, The in-plane free vibration of an elastically supported thin ring rotating at high speeds revisited, J. Sound Vib. 402 (2017) 203–218.
[3] S. Gong, Tire Ring Model: Literature Review, Technical Report, Technische Universiteit Delft, 1989.
[4] H. Xu, D. Qin, Vibration characteristics of flexible spur ring gears using different connection types, J. Low Freq. Noise Vib. Act. Control 39 (2019) 146134841984202.
[5] S.-Y. Wang, C. Meesap, Investigation on mesh and sideband vibrations of helical planetary ring gear using structure, excitation and deformation symmetries, Chin. J. Mech. Eng. 31 (1) (2018) 104.
[6] L.F. Braña, H. Campelo, X.M. López-Fernández, Quiet transformers: Design issues, in: Advanced Research Workshop on Transformers, ARWtr, 2013, http://dx.doi.org/10.13140/2.1.2620.0962.
[7] M. Jin, Y. Wang, J. Pan, Vibration of circular rings coupled by elastic elements, Appl. Acoust. 148 (2019) 264–275.
[8] A. Love, A Treatise on the Mathematical Theory of Elasticity, vol. 1, 1892.
[9] S. Rao, Vibration of circular rings and curved beams, in: Vibration of Continuous Systems, John Wiley & Sons, Inc, 2007, pp. 393–407.
[10] J. Kirkhope, Out-of-plane vibration of thick circular ring, J. Eng. Mech. Div. 102 (2) (1976) 239–247.
[11] A. Bhimaraddi, P. Moss, A. Carr, Out-of-plane vibrations of thick rings, Thin-Walled Struct. 8 (1) (1989) 73–79.
[12] C. Tang, C. Bert, Out-of-plane vibrations of thick rings, Int. J. Solids Struct. 23 (1) (1987) 175–185.
[13] W. Bickford, S. Maganty, On the out-of-plane vibrations of thick rotating rings, J. Sound Vib. 110 (1) (1986) 121–127.
[14] I. Senjanovic, I. Ćatipović, N. Alujević, D. Čakmak, N. Vladimir, Free in-plane and out-of-plane vibrations of rotating thin ring based on the toroidal shell theory, Arch. Mech. 70 (2018) 429–455.
[15] S. Vidoli, F. dell'Isola, Modal coupling in one-dimensional electromechanical structured continua, Acta Mech. 141 (1–2) (2000) 37–50.
[16] S.U. Benscoter, R.H. MacNeal, Introduction to Electrical-Circuit Analogies for Beam Analysis, Technical Report, 1952.
[17] S.U. Benscoter, R.H. MacNeal, Equivalent-Plate Theory for a Straight Multicell Wing, Technical Report, 1952.
[18] R.H. MacNeal, Electrical Analogies for Stiffened Shells with Exible Rings, Technical Report, NACA, 1954.
[19] R.H. MacNeal, Electric Circuit Analogies for Elastic Structures, in: Airplane, missile and spacecraft structure series, John Wiley & Sons Canada, Limited, 1962.
[20] S. Alessandroni, F. dell'Isola, M. Porfiri, A revival of electric analogs for vibrating mechanical systems aimed to their efficient control by PZT actuators, Int. J. Solids Struct. 39 (20) (2002) 5295–5324.
[21] F. dell'Isola, M. Porfiri, S. Vidoli, Piezo-Electromechanical (PEM) structures: Passive vibration control using distributed piezoelectric transducers, C. R. Méc. 331 (1) (2003) 69–76.
[22] M. Porfiri, F. dell'Isola, F.M. Frattale Mascioli, Circuit analog of a beam and its application to multimodal vibration damping, using piezoelectric transducers, Int. J. Circuit Theory Appl. 32 (4) (2004) 167–198.
[23] S. Alessandroni, U. Andreaus, F. dell'Isola, M. Porfiri, A passive electric controller for multimodal vibrations of thin plates, Comput. Struct. 83 (15) (2005) 1236–1250.
[24] S. Alessandroni, U. Andreaus, F. dell'Isola, M. Porfiri, Piezo-electromechanical (PEM) Kirchhoff-Love plates, Eur. J. Mech. A Solids 23 (4) (2004) 689–702.
[25] B. Lossouarn, M. Aucejo, J.-F. Deü, K.A. Cunefare, Design of a passive electrical analogue for piezoelectric damping of a plate, J. Intell. Mater. Syst. Struct. 29 (7) (2018) 1301–1314.
[26] B. Lossouarn, J.-F. Deü, M. Aucejo, Multimodal vibration damping of a beam with a periodic array of piezoelectric patches connected to a passive electrical network, Smart Mater. Struct. 24 (11) (2015) 115037.
[27] B. Lossouarn, M. Aucejo, J.-F. Deü, Multimodal coupling of periodic lattices and application to rod vibration damping with a piezoelectric network, Smart Mater. Struct. 24 (4) (2015) 045018.
[28] R. Darleux, B. Lossouarn, I. Giorgio, F. dell'Isola, J.-F. Deü, Electrical analogs of curved beams and application to piezoelectric network damping, Math. Mech. Solids 27 (4) (2022) 578–601.
[29] A. Luo, B. Lossouarn, A. Erturk, Analogous piezoelectric network for multimodal vibration attenuation of a thin circular ring, Smart Mater. Struct. 32 (11) (2023) 115024.
[30] A. Labuschagne, N. van Rensburg, A. van der Merwe, Comparison of linear beam theories, Math. Comput. Modelling 49 (1) (2009) 20–30.
[31] I. Elishakoff, Handbook on Timoshenko-Ehrenfest Beam and Uflyand-Mindlin Plate Theories, World Scientific, Singapore, 2020, http://dx.doi.org/10.1142/10890.
[32] A. Luo, B. Lossouarn, A. Erturk, The effects of shear deformation and rotary inertia on the electrical analogs of beams and plates for multimodal piezoelectric damping, Int. J. Circuit Theory Appl. (2023).
[33] J. Lin, W. Soedel, On general in-plane vibrations of rotating thick and thin rings, J. Sound Vib. 122 (3) (1988) 547–570.
[34] Z. Liu, F. Zhou, C. Oertel, Y. Wei, Three-dimensional vibration of a ring with a noncircular cross-section on an elastic foundation, Proc. Inst. Mech. Eng., Part C: J. Mech. Eng. Sci. 232 (13) (2018) 2381–2393.
[35] G. Raze, J. Dietrich, B. Lossouarn, G. Kerschen, Shunts vs networks: Tuning and comparison of centralized and decentralized piezoelectric vibration absorbers, Smart Mater. Struct. 31 (11) (2022) 115006.
[36] Y. Zheng, W. Tian, N.K.X. Lee, Y. Qu, G. Meng, A programmable macro-fiber-composite meta-ring with digital shunting circuits, J. Sound Vib. 533 (2022) 117017.
[37] S. Dong, C. Alpdogan, E. Taciroglu, Much ado about shear correction factors in Timoshenko beam theory, Int. J. Solids Struct. 47 (13) (2010) 1651–1665.
[38] J. Kirkhope, In-plane vibration of a thick circular ring, J. Sound Vib. 50 (2) (1977) 219–227.
[39] S.K. Ugural, Advanced Strength and Applied Elasticity, American Elsevier Pub. Co., New York, 1975.
[40] M. Paschero, Modeling and Synthesis of Circuits Analogue to Generalized Ondulatory Phenomena Giroscopically Coupled (Ph.D. thesis), 2007.
[41] S. Rao, A. Prasad, Vibrations of annular plates including the effects of rotatory inertia and transverse shear deformation, J. Sound Vib. 42 (3) (1975) 305–324.
[42] R. Bhagat, M. Amateau, C. Smith Edward, Damping behavior of mechanically alloyed aluminum and aluminum matrix composites, Int. J. Powder Metall. 25 (4) (1989) 311–316.
[43] B. Lossouarn, G. Kerschen, J.-F. Deü, An analogue twin for piezoelectric vibration damping of multiple nonlinear resonances, J. Sound Vib. 511 (2021) 116323.